

Continuous Shear Roll Milling of Gun Propellants*

Dilhan M. Kalyon and Halil Gevgilili,

Stevens Institute of Technology, Castle Point St., Hoboken, NJ 07030

The continuous shear roll milling can be used for the processing and granulation of gun propellants. Here a mathematical model of the continuous shear roll milling process will be presented along with experimental data collected on live and simulant propellant formulations. The role of the flow boundary condition will be shown to be critical in the processability analysis. The safety aspects will be discussed under the light of the modeling and experimental results.

** The complete manuscript will be submitted to Journal of Energetic Materials*

Introduction

Various roll-driven operations including calendering, roll milling, and continuous shear roll milling processes can be used for processing of propellants. In these processes the propellant is pressurized and forced into the nip region between two rolls rotating at the same or different speeds. The sticking of the melt to one or both rolls and the eventual detachment of the polymer melt from one or both rolls define the processability window of the propellant formulation in such processes. Among these roll-driven processes the continuous shear roll milling process [1-4] is especially useful for the processing of various types of propellants.

The shear roll extruder involves two heated counter-rotating rolls with grooves built into them (Figure 1). The rolls typically have different roughnesses and are run at different temperatures and/or rotational speeds. The fundamental steps of the processing operation of the propellant are:

1. Conveying and compaction of the feed material
2. The melting of the binder if a thermoplastic binder is used
3. The squeezing out and the evaporation of the water
4. The dispersion and homogenization of the felt
5. Cutting and granulation

Experimental Equipment, Procedures and Observations

Two different types of shear roll milling equipment were used in the project. First, a pilot scale shear roll mill was designed and built for the shear roll milling experiments (Figure 1). This pilot scale shear roll mill had two 75 mm rolls and they were powered by two separate electrical drives with motor ratings of 2 HP and which could rotate at different rotational speeds. This shear roll mill was used with simulants to understand the basic flow and heat transfer mechanisms of the process. In these experiments inert polymeric pellets were fed into the gap between the two rolls using an Acrison gravimetric feeder.

The front roll, “feed roll”, has a rougher surface and the melt typically continuously adheres only to the feed roll as a result of its higher surface roughness for similar feed and conveying roll temperatures. In our experimental equipment the feed roll contained two heat transfer zones controlled by the circulation of a heat transfer medium, i.e., typically a thermostatted silicone oil. The first zone is adjacent to the feed end and the second heat transfer zone is located adjacent to the scraper end, at which the polymer is removed from the shear roll mill. A higher temperature is generally used at the first temperature control zone in comparison to the second temperature control zone of the feed roll to give rise to the faster melting of the polymer and to initiate stick to the conveying roll surface. There is only one temperature control zone in the conveying roll.

Under typical operating conditions, the material wraps around the feed roll and is in contact with the second “conveying “ roll at the nip region between the two rolls. Thus under steady state processing conditions, the melt typically periodically sticks and then detaches from conveying roll every time it goes through the nip region, whereas the melt continuously sticks to the feed roll. Furthermore, the temperature of the feed roll is typically set higher than the temperature of the conveying roll. This guarantees the adhesion of material to feed roll.

When both roll temperatures are identical, the melt continuously sticks to only the feed roll. However, our experiments with polyethylene revealed that if the temperature of the conveying roll is set approximately 17°C higher than the feed roll for this polymer, the melt sticks onto the conveying roll in spite of its smoother surface. At slightly lower temperatures the process may become unstable and the melt can switch the roll onto which it continuously sticks. Overall, a combination of the surface roughness and the temperature difference on the two rolls determines the roll onto which the melt continuously sticks.

The principal parameters of our experimental study were the rotational speeds of the feed and conveying rolls. The mass flow rate, the gap between the rolls and the temperatures of the rolls were held constant (the two rolls were kept at the same temperature). An

Inframetrics Thermacam PM 290 thermal imaging camera was employed during these experiments to determine the surface temperature distribution of the rolls prior to the initiation of the extrusion process and the temperature distribution of the melt at its free surface as a function of location during the experiments. The thermal imaging camera has a working range of -10 to 450 °C and an accuracy of ± 0.2 °C. Thermonitor 95 Pro remote analysis software was used for the collection and analysis of the thermal images. The typical distribution of the temperature of the melt during the process indicates that the temperature of the melt is kept within a narrow range from the inlet to the exit of the shear roll milling process. The oil temperatures in the two rolls were set differently to achieve the reported roll surface temperatures. The emissivity values of the two surfaces were determined and were used in the temperature determination.

Upon reaching steady state for each run (as evidenced by steady state temperature distributions of the melt with the thermal imaging camera), we performed a pulse-input tracer residence time distribution experiment. For the pulse-incorporation of the tracer, we injected pulses consisting of a simulant with a carbon black tracer into the feed and recorded the progress of the color tracer using a digital video camera. The carbon black tracer did not spread significantly in the axial direction but rather formed relatively narrow rings, the width of which did not increase substantially in the axial direction, suggesting that the backmixing occurring in the shear roll mill is limited. Since there is no barrel, the shear roll mill conveys the material forward only through the intervention of the second roll. The nip region allows the material between the two rolls to be pressurized and conveyed, as if it were processed in a calender and followed by a whole revolution during which no further deformation takes place. Upon reaching the next nip region the material is once again deformed, pressurized, back-mixed, generates new free surfaces and is conveyed forward. On our 85 mm pilot-scale shear roll mill this corresponds to 200 passages through the nip region.

After the completion of various experiments, we simultaneously brought both rolls to a complete stop “dead-stop” and measured the wall thickness of the film at ambient temperature and hence the weight distribution under steady flow or at the point that the

unstable flow is initiated as evidenced through the detachment of the polymer melt from both rolls. The data suggest that the conveying capability of the shear roll mill changes with the operating conditions used. Typically, the increased roll speeds give rise to increased conveying capability as indicated by the reduced thickness of the material on the rolls and hence a reduced mean residence time during the process.

Processing of live gun propellant

A second set of experiments were carried out using a shear roll mill with roll diameters of 200 mm in conjunction with a live gun propellant. The overall length of the rolls are around 130 cm and thus generate a length over diameter ratio of 130/20, i.e., 6.5. The rolls are heated in a multi zone arrangement. The gap between the two rolls can theoretically be set but as our experiments have shown in reality the gap cannot be controlled precisely. The propellant is fed into the gap between the two rolls. The container at the bottom indicates that some of the material does not stick to the rolls and falls immediately to the bottom. With the manufacturing scale shear roll mills, one of the rolls is polished (back) and the other is roughened (front). Both rolls have grooves built into them, with the helix angle of the grooves remaining constant from one end of the shear roll mill to the end. At the granulator end the grooves on the rolls run out and the propellant is forced to flow into a sieve followed by a cutter.

We have used two thermal cameras and two video cameras during the operation of the shear roll mill with the live propellant formulation. The thermal cameras were connected to two laptop computers. We have used remote control software for the collection of the thermal images as the experiments took place.

The live propellant felt on the back roll during the operation is shown in Figure 2. During the experiments with the live propellant it was determined that:

- a. The propellant felt is not evenly distributed on the rolls. There seems to be a lot of material in the nip region, and the volume of material is the greatest at locations not directly at the feed zone but at the intermediary locations between the feed and the mid-point of the length of the shear roll mill.

- b. The amount of material in the nip region appears to decrease with increasing distance in the down-channel direction.
- c. The felt does not stick well to the roll surface in the feed section. The stick condition is generally observed as one moves in the down-channel direction.
- d. The felt only sticks to the front roll and not to the back roll.
- e. There seems to be a lot of air encapsulated in the felt especially in the nip region, where the felt is pleated and folds back on itself repeatedly (see Figure 3).
- f. The felt initially does not stick well to the surface of the roll.
- a. There are pockets of water vapor, which can be seen from the deformation of the felt surface. This should be a result of the vaporization of the water at the surface of the rolls and its encapsulation by the presence of the felt and the lack of a mechanism for the diffusion of the water vapor out of the felt (limited by the solubility of the water vapor in the felt).
- b. The felt is compressed at the nip region with pockets of air also squeezed (see Figures 2, 3). This may generate an adiabatic compression problem if the air pocket is squeezed relatively fast and the air pocket is relatively large with no pathway for the air to escape. It is also seen how difficult it is for the felt to be squeezed in the nip region, suggesting that significant forces need to be applied for the gun propellant to be forced into the nip area.
- c. The forward motion of the felt is controlled by the deformation occurring at the nip.
- d. The roughness of the rolls and the roll temperatures are important because they control the slip/stick behavior of the felt on the rolls.
- e. Without the sticking of the material onto the rolls there is no mechanism for forward motion and the generation of viscous energy dissipation on a material which is not moving forward will lead to rapid moisture loss and the burning of the propellant.

During the live runs, the screw rotational speeds could be kept at the targeted values. The typical roll speeds were 42 rpm for the front and 35 rpm for the back roll. This difference in the screw speeds is another important aspect of the shear roll mill process.

The front roll (which holds the felt) generally is rotated at a faster speed than the back roll which is used to pressurize and move the material in the forward direction. On the other hand the temperature of the front roll is always greater than the back roll. This again makes sense since the felt should stick to the hotter surface and slip away from the colder surface. There is a significant difference (over 20 °C) between the temperatures on the feed roll and the surface temperatures of the conveying roll (Figure 4). The torques on the front and the back rolls were also measured and suggested that the torque on the front roll was greater than on the back roll. Figure 4 also indicates that following the settings the feed end of the rolls are at a greater temperature in comparison to the granulator (exit) end of the shear roll mill. During the run the temperature of the propellant felt increases asymptotically with time. The rate of change of temperature with time is relatively high at the beginning of the run but slows down sufficiently so that a steady state can be assumed after 10-15 minutes of operation (Figure 4 provides the steady state condition). The temperature of the felt increases from the feed section to the granulation section of the rolls. Furthermore, the temperature distribution results indicate that the surface temperatures of the rolls are less than the set values at the beginning of the runs.

Process Analysis: Mathematical Modeling of the Shear Roll Mill Process using 1-D Model and Macroscopic Energy Balance

It is possible to carry out the numerical analysis of the flow dynamics especially using FEM [5-11] but an analytical analysis using the lubrication flow assumption is preferable at the outset to better understand the relationship between various parameters and their effects on the thermo-mechanical history which is generated during the process. The analysis of the shear roll mill process can be simplified considerably if the forward motion of the material in a shear roll extruder is neglected. This is generally justified because the forward velocities of the melt are a couple of orders of magnitude smaller than the roll velocities

It is the interface between the two rolls, which moves and translates the felt in the forward direction and generates the compression and the pressurization of the felt, and the squeezing out of its water. The nip area also allows some degree of back-mixing during which the material is circulated and new free surface is generated allowing the water vapor to be released to the environment. Overall, only heat transfer is important during the travel of the felt from one nip region to the other. The velocity distribution is known (identical to the radial velocity of the feed roll) and is flat at the point that the felt is detached from the rolls. The velocity distribution changes significantly as a function of distance in the down-channel direction when the felt is in between the two rolls.

The model that will be used here is based on the general treatise along those of Gaskell and McKelvey [12-17]. In this analysis the flow is assumed to be laminar, incompressible, quasi isothermal and laminar. The rolls have a radius of R and rotate in opposite directions with frequency of rotation of N . The minimum nip separation is H_0 and the material is distributed laterally over a distance of W , which spans the distance from $x=X_2$, where the rolls bite into the material upstream to $x=X_1$, where the material detaches from the conveying roll downstream, $x=0$ being the point of minimum gap separation. Hence, W is equal to sum of X_1 and X_2 . The pressure is atmospheric at X_1 and X_2 . The distance of separation between the rolls to radius H/R is assumed to be small, which enables us to assume that the velocity profile at any location x is considered identical to the velocity profile between two parallel plates, which are $2h$ distance apart. The equations of continuity and momentum will reduce to:

$$\frac{dv_x}{dx} = 0 \quad (1)$$

$$\frac{\partial P}{\partial x} = \frac{\partial \tau_{yx}}{\partial y} = \mu \frac{\partial^2 v_x}{\partial y^2} \quad (2)$$

with the boundary conditions, $v_x(\pm h)=U$ where, U is the tangential velocity of the roll surfaces, $U=2\pi NR$ and $\pm h$ correspond to the two roll surfaces. The distance $2h$ between the two rolls changes in the nip as the material travels down stream. The functional

relationship between h and x , at any downstream location between X_1 and X_2 is (Figure 5):

$$h = H_0 + R - \sqrt{R^2 - x^2} \quad (3)$$

The momentum equation can be rearranged to

$$\frac{dP}{dx} = \frac{3\mu U}{H_1^2} \left(1 - \frac{H_1}{h}\right) \left(\frac{H_1}{h}\right)^2 \quad (4)$$

where, h equals to H_1 at $x=X_1$. This equation implies that the pressure gradient is zero at X_1 , at the detachment point, where the pressure drops to atmospheric pressure and at X_1 , somewhere upstream from the minimum gap separation point, where the pressure attains a maximum.

Using binomial expansion, Equation 3 can be approximated to

$$\rho^2 = \frac{x^2}{2RH_0} \quad (5)$$

At $x=X_1$ and $-X_1$, i.e. at the detachment and maximum pressure points

$$\lambda^2 = \frac{X_1^2}{2RH_0} \quad (6)$$

With these definitions and approximations it is possible to integrate Equation 4 to the following form

$$P = \frac{3\mu U}{4H_0} \sqrt{\frac{R}{2H_0}} \left\{ \left[\frac{\rho^2 - 1 - 5\lambda^2 - 3\lambda^2\rho^2}{(1 + \rho^2)^2} \right] \rho + (1 - 3\lambda^2) \tan^{-1} \rho + C(\lambda) \right\} \quad (7)$$

with the integration constant being

$$C(\lambda) = \frac{(1 + 3\lambda^2)}{(1 + \lambda^2)}\lambda - (1 - 3\lambda^2)\tan^{-1}\lambda \quad (8)$$

Similarly starting from the continuity equation it is possible to obtain the velocity profile as:

$$u_x = 1 + \frac{3(1 - \xi^2)(\lambda^2 - \rho^2)}{2(1 + \rho^2)} \quad (9)$$

where u_x is the velocity normalized with respect to the roll velocity, i.e. v_x/U and ξ is the dimensionless gap y/H . Finally, knowing the velocity profile it possible to get the shear rate distribution as:

$$\dot{\gamma}_{yx}(\xi) = \frac{3U(\rho^2 - \lambda^2)}{H_0(1 + \rho^2)^2}\xi \quad (10)$$

Using this relationship one can evaluate the viscous energy dissipation term within the nip, which needs to be utilized in the macroscopic energy balance (Figure 5). In the nip region some typical velocity and shear rate profiles calculated using the 1-D calendering equations are shown in Figure 6. The negative velocity is indicative of the back-mixing to occur at the entrance to the nip region. It should be noted that the Newtonian fluid assumption is a significant limitation since it is known that the shear viscosity of the felt, η , is not a constant but a material function which will vary as:

$\eta = f(\text{shear rate, temperature, water concentration, degree of homogenization of the felt})$

Under the scope of this study, it was not possible for us to characterize the shear viscosity material function of the felt as a function of temperature, shear rate, water and degree of homogenization. The macroscopic energy balance over a ring of felt is shown in Figure 6:

$$\begin{aligned}
Q\rho c_p (T_{\text{out}} - T_{\text{in}}) = & 2\pi(R + H_1)\Delta Lh(T_{\text{air}} - T_{\text{felt}}) + k \frac{(T_{\text{roll}} - T_{\text{felt}})}{H_1} 2\pi(R)\Delta L \\
+ [\mu\dot{\gamma}_{xy}^2 + 2\mu\dot{\gamma}_{xx}^2] \Delta V_{\text{nip}} - & \Delta H_{\text{water}} Q(X_{w-\text{in}} - X_{w-\text{out}})
\end{aligned} \tag{11}$$

The term on the left hand side of the equation is the energy accumulation term representing the temperature change. The first term on the right hand side is energy transferred from the felt to the surrounding air by free or forced convection, the second term represents the heat conduction from the roll surface to the felt, the third term stands for the viscous energy dissipation upon shearing and extension in the nip region and the last term accounts for the heat loss due to water evaporation. The volume of propellant found in the nip region is designated by ΔV_{nip} .

The macroscopic energy balance is integrated by finite differences method. The thickness of the control volume as of Figure 6 (over which the macroscopic balance was performed) was reduced gradually, until the results were independent of the density of the finite difference grid. The typical velocity and the shear rate distributions for one particular run during the experiments with the live formulation are shown in Figures 7 and 8.

The comparison of the temperature of the felt which is measured and which is determined using the macroscopic balance is shown in Figure 9. The corresponding losses of water as a function of distance in the shear roll mill are also shown in Figure 10. The results suggest that the overall mechanisms assumed are relevant since a few adjustable parameters are sufficient to represent the entire behavior of the felt from the feed to the granulation sections. The only mismatch occurs in the hopper area. It is likely that some stagnant amount of propellant discovered during the tracer experiments is responsible for the noted discrepancy. The rate of water loss is initially high and decreases as the concentration of the water is reduced.

The variation of the water content with temperature is shown in Figure 10. The water concentration decreases with increasing average material temperature. The shear viscosity increases with decreasing water content. Overall, the results indicate that under various conditions the conditions can give rise to appreciable decrease of the water content followed by increase of the viscous energy dissipation and then the increase of the temperature to above the decomposition temperature of the propellant. Such conditions can thus be determined apriori and eliminated from the processing operation to minimize the safety risk of the process.

Acknowledgements:

This work was supported by TACOM/ARDEC under contract DAAE30-01-C-1039. We are grateful for this support. We acknowledge with gratitude the contributions of Mr. James E. Kowalczyk and Mr. James B. Graybill of MPR Inc. of Hackensack, New Jersey in the design and the manufacturing of the shear roll mill used in the experimental study. We also thank M. Malik, H. Tang, T. Kiryaman, H. Filiz of Stevens and Messers. C. Topolski, S. Rosenberg, D. Fair, A. Perich, W. Miller, N. Campesi, E. Krajkowski (ARDEC), Dr. Hays Zeigler of ATK Systems of Radford, VA, and Dr. A. Wellm of NitroChemie, Germany. We further thank the staff of NitroChemie for the diligent help they provided to our experimental program.

References:

1. Menges, G., Krueger, E., "Compounding of PVC," *Kunststoffe* 75, 5 (1985).
2. Berghaus, U., Bartilla, T., Heidemeyer, P., Crolla, G., "Polymerisation und Blendherstellung, Teil 3: Kontinuierliches Mischen von Polyvinylchlorid (Polymers and blends. Part 3: Continuous mixing of polyvinyl chloride)," *Plastverarbeiter* 39 (1988).
3. Albers, A., "Compounding with a shear roll extruder a new proces for plastication and dispersion of highly viscous materials," *Kunststoffe* 82, 10 (1992).
4. Albers, A., "Aufbereitung von Galvanik- und Lackschlaemmen mit kontinuierlichem Scherwalzentrockner," *Galventchnik* 85, 6 (1994).
5. Kiparissides, C., Vlachopoulos, J., "Finite element analysis of calendaring," *Polymer Engineering and Science* 16, (1976).
6. Kiparissides, C., Vlachopoulos, J., "Study of viscous dissipation in the calendaring of power-law fluids," *Polymer Engineering and Science* 18 (1978).
7. Levine, L., Corvalan, C. M., Campanella, O. H., Okos, M. R., "A model describing the two-dimensional calendaring of finite width sheets," *Chemical Engineering Science* 57 (2002).
8. Klostermann, R., Von Bose, S., Mewes, D., "Comparison of calculated with measured flow fields in the gap between two rotating rolls," *Advances in Polymer Technology* 13, 3 (1994).
9. Agassant, J. F., Espy, M., "Theoretical and experimental study of the molten polymer flow in the calender bank," *Polymer Engineering and Science* 25 (1985).
10. Ng T. S., Angerer G., "Estimation of the shear deformation exerted by a roll-mill upon a rubber compound," *Polymer Engineering and Science* 20, 8 (1980).
11. Yao, C. H, Manas-Zloczower, I., "Study of mixing efficiency in roll-mills," *Polymer Engineering and Science* 36, 3 (1996).
12. McKelvey, J.: *Polymer processing*. John Wiley and Sons, (1962)
13. Middleman S.: *Fundamentals of polymer processing*. McGraw Hill Book Company, New York (1977).

14. Tadmor, Z., Gogos, C.: Principles of polymer processing. John Wiley and Sons, New York (1979).
15. Gaskell, R.,” The Calendering of Plastic Materials,” J. Appl. Mech. 17 (1950).
16. Allston, W., Astill, K.,”An analysis for the calendaring of non-Newtonian fluids,” J. Appl. Polym. Sci. 17 (1973).
17. Brazinsky, I., Cosway, H. F., Valle, C. F., Jones, R. C.,” A theoretical study of liquid-film spread heights in the calendaring of newtonian and power law fluids,” J. Appl. Polym. Sci. 14, 11 (1970).
18. D. Kalyon, H. Gevgilili and A. Shah, “Detachment of the polymer melt from the roll surface: data from a shear roll extruder”, International Polymer Processing, 19, 2, 129-138 (2004).

List of Figures:

Figure 1: The basic features of the shear roll mill

Figure 2: The live propellant felt on the back roll during the operation.

Figure 3: Air is encapsulated in the felt especially in the nip region, where the felt is pleated and folds back on itself repeatedly.

Figure 4: Typical roll temperature profiles prior to a run

Figure 5: Schematic drawing of the nip region of the shear roll mill and the velocity profiles for similar roll speeds.

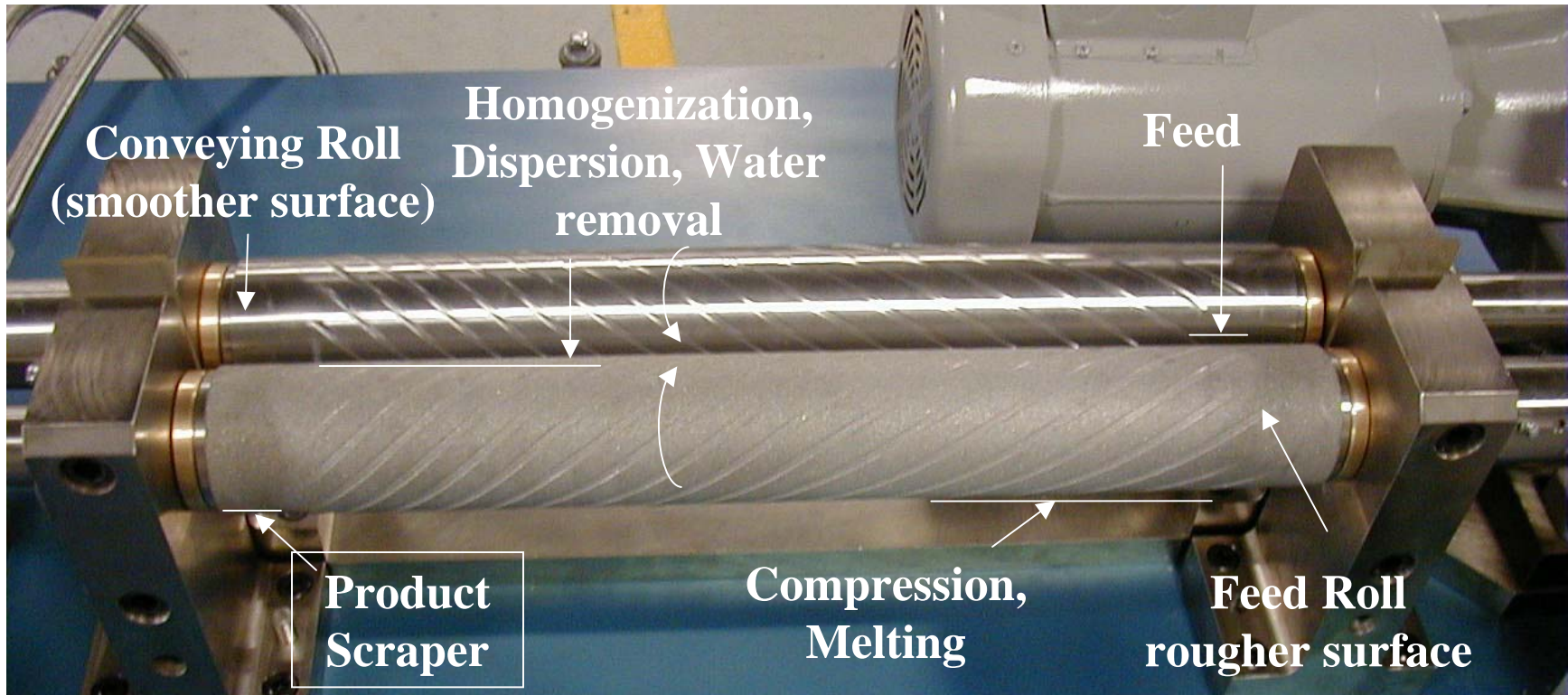
Figure 6: Macroscopic Energy Balance on a strip of material.

Figure 7: Dimensionless velocity profile of the material at various points along the nip

Figure 8: Shear rate profile within the nip.

Figure 9: Experimental and predicted temperature profile along the rolls under following conditions: Flow rate=45 kg/hr, feed roll speed=45 rpm, conveying roll speed 38 rpm, set temperature of the at the inlet section of the feed roll=120°C, set temperature of the at the discharge section of the feed roll=105°C, set temperature of the at the conveying roll=90°C.

Figure 10: Predicted moisture level along the rolls under following conditions: Flow rate=45 kg/hr, feed roll speed=45 rpm, conveying roll speed 38 rpm, set temperature of the at the inlet section of the feed roll=120°C, set temperature of the at the discharge section of the feed roll=105°C, set temperature of the at the conveying roll=90°C.



The basic features of the shear roll mill

Figure 1

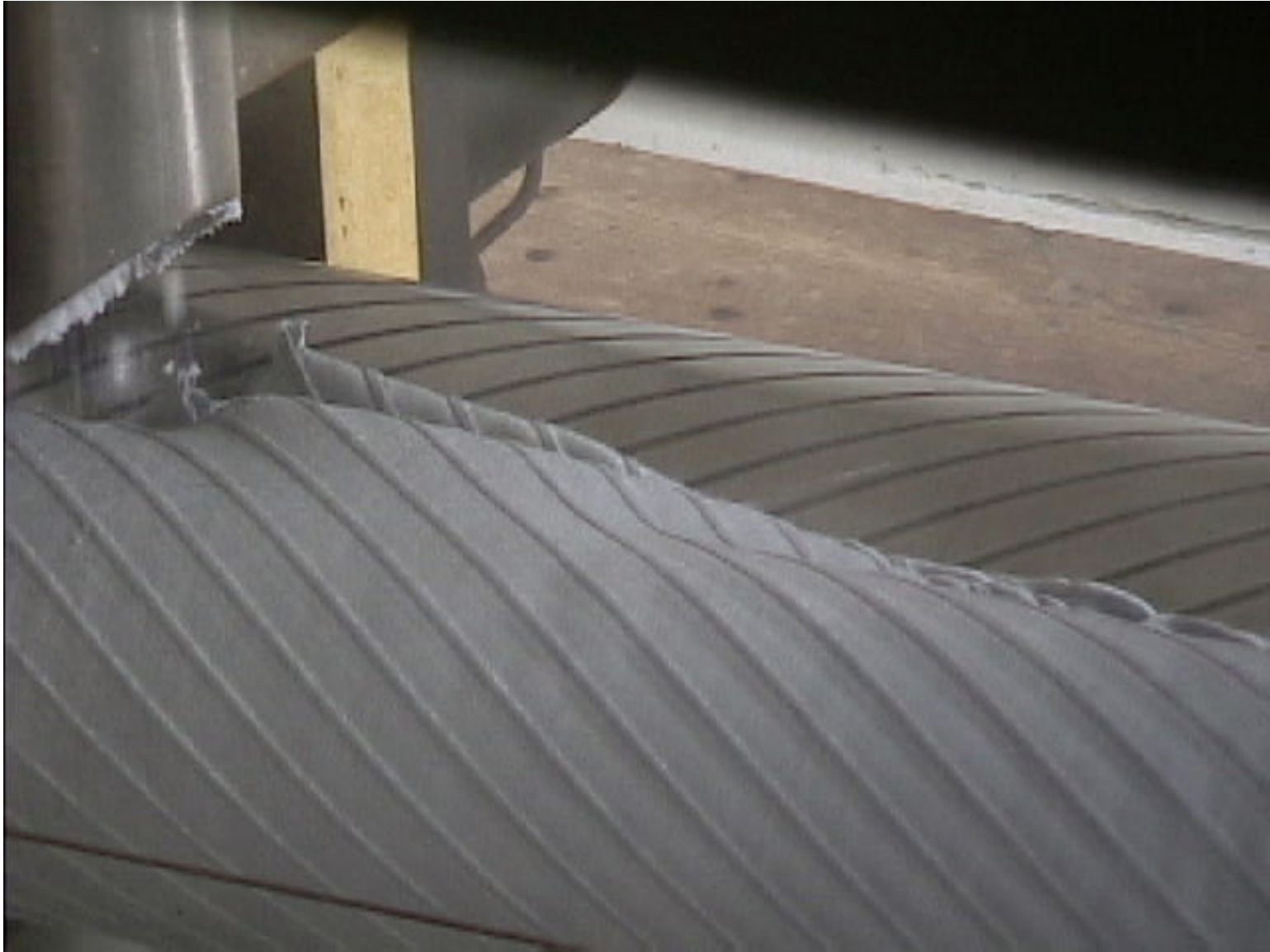


Figure 2



Figure 3

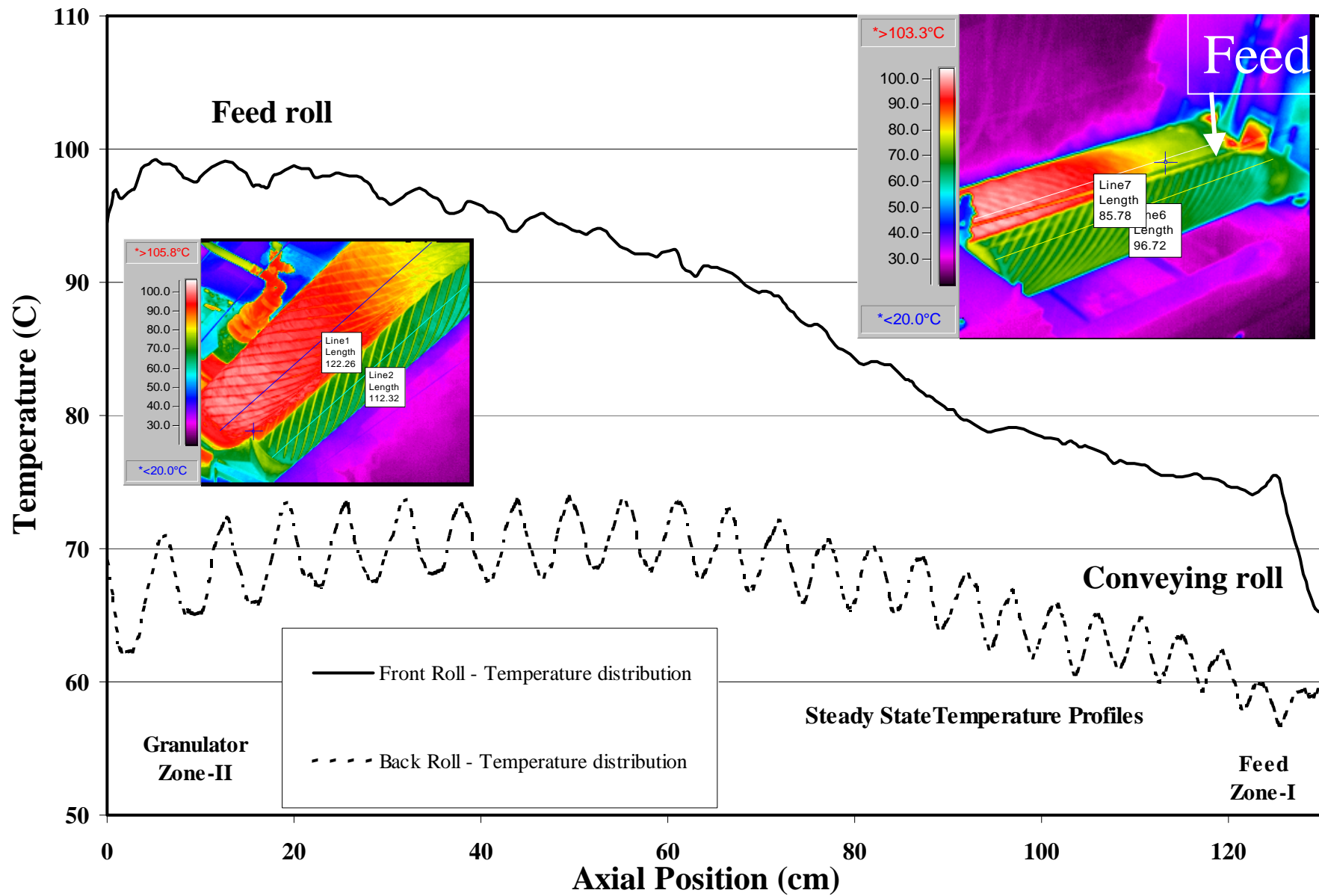


Figure 4

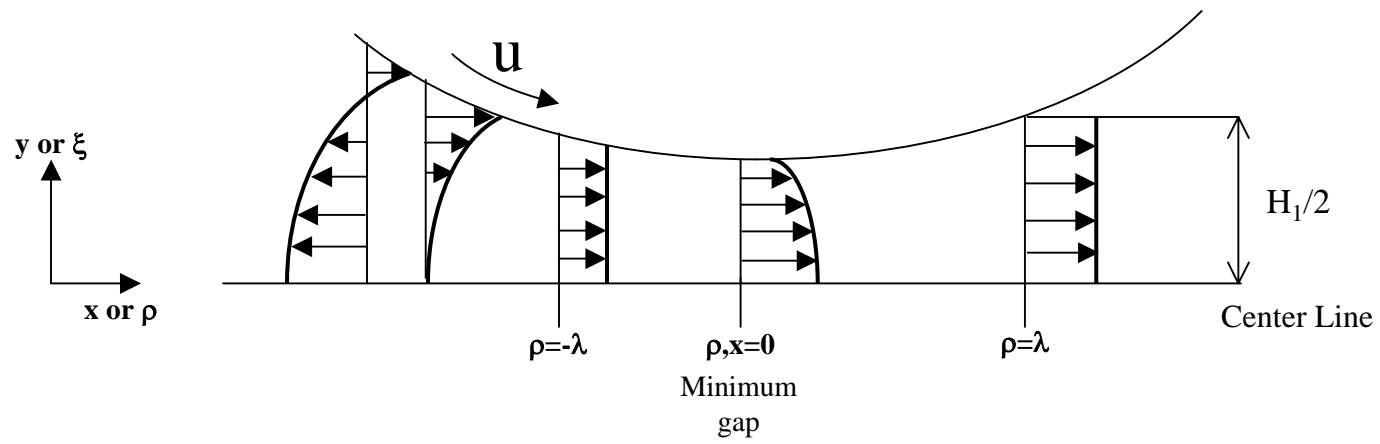


Figure 5

$$Q\rho c_p (T_{out} - T_{in}) = 2\pi(R + H_1)\Delta Lh(T_{air} - T_{felt}) + k \frac{(T_{roll} - T_{felt})}{H_1} 2\pi(R)\Delta L$$

$$+ \left[\mu \dot{\gamma}_{xy}^2 + 2\mu \dot{\gamma}_{xx}^2 \right] \Delta V_{nip} - \Delta H_{water} Q(X_{w-in} - X_{w-out})$$

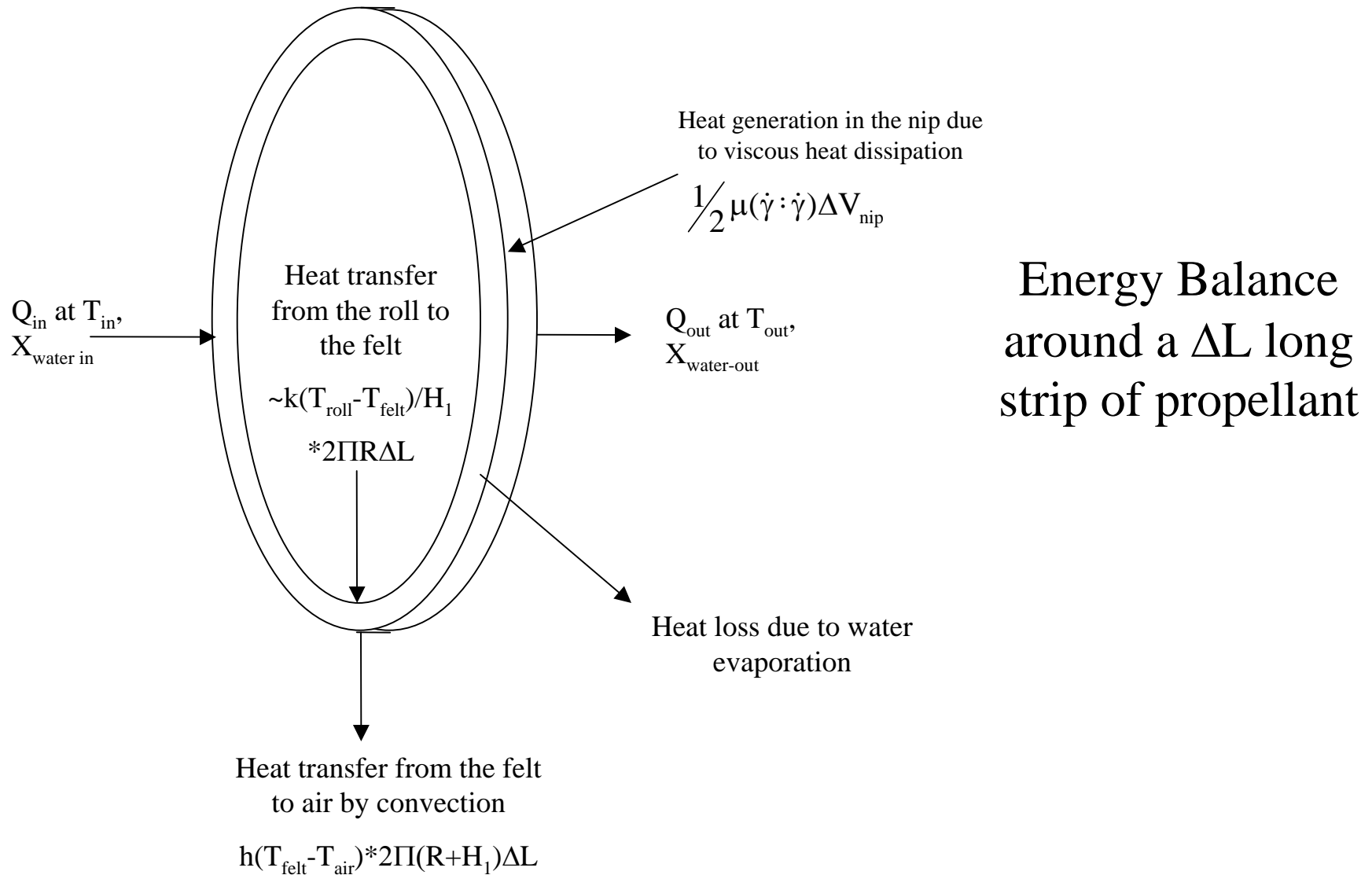


Figure 6

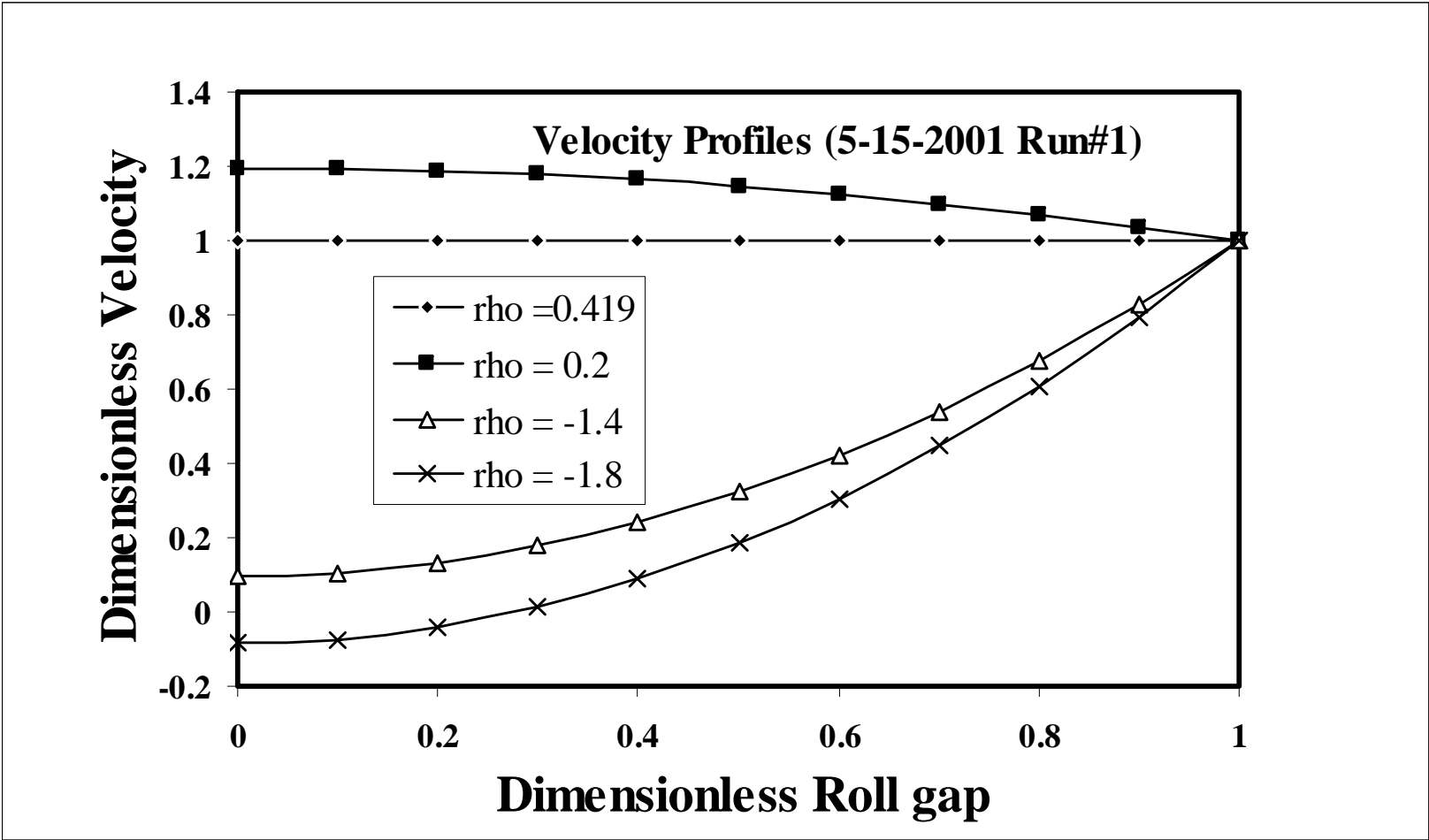


Figure 7

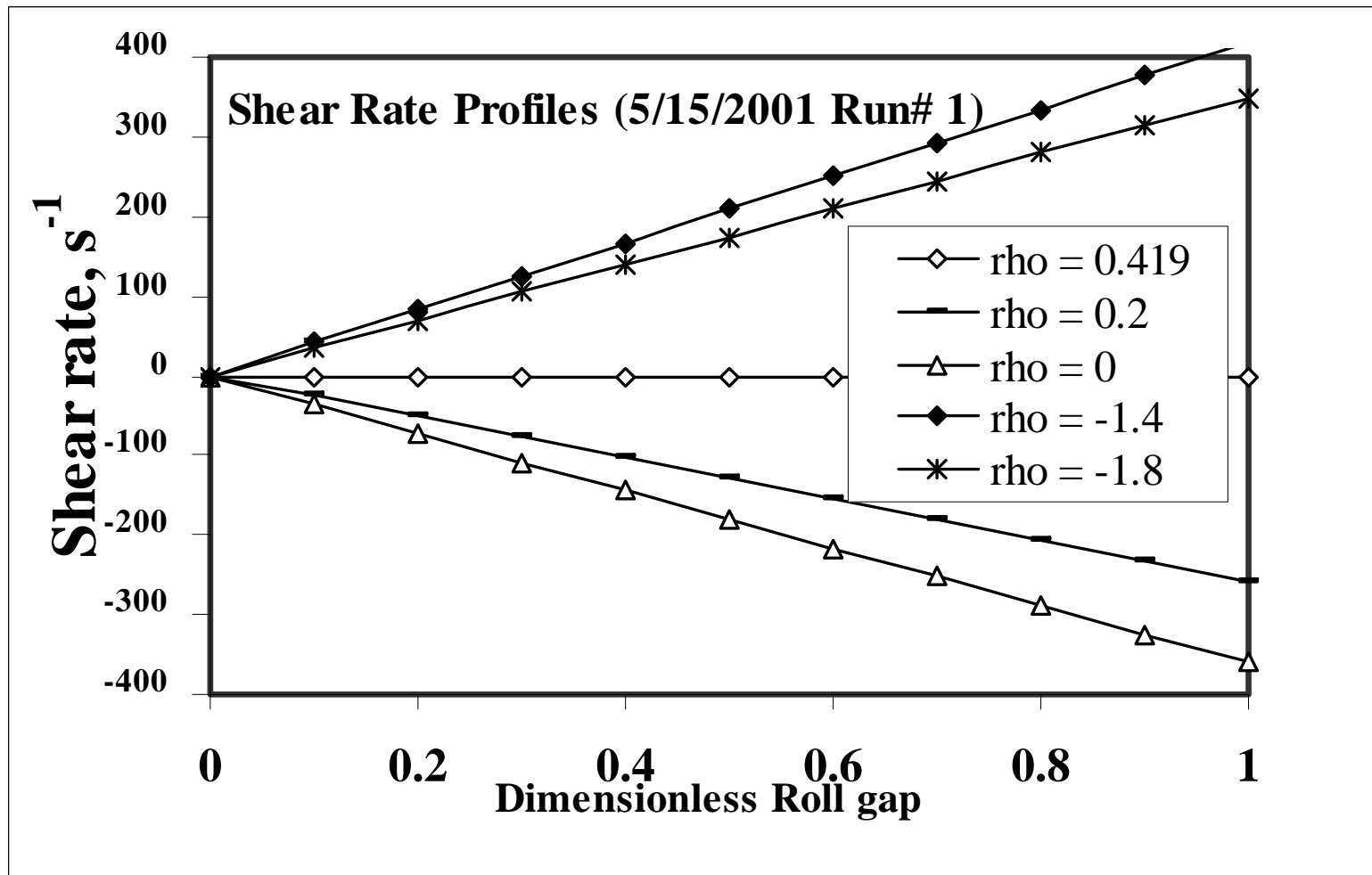


Figure 8

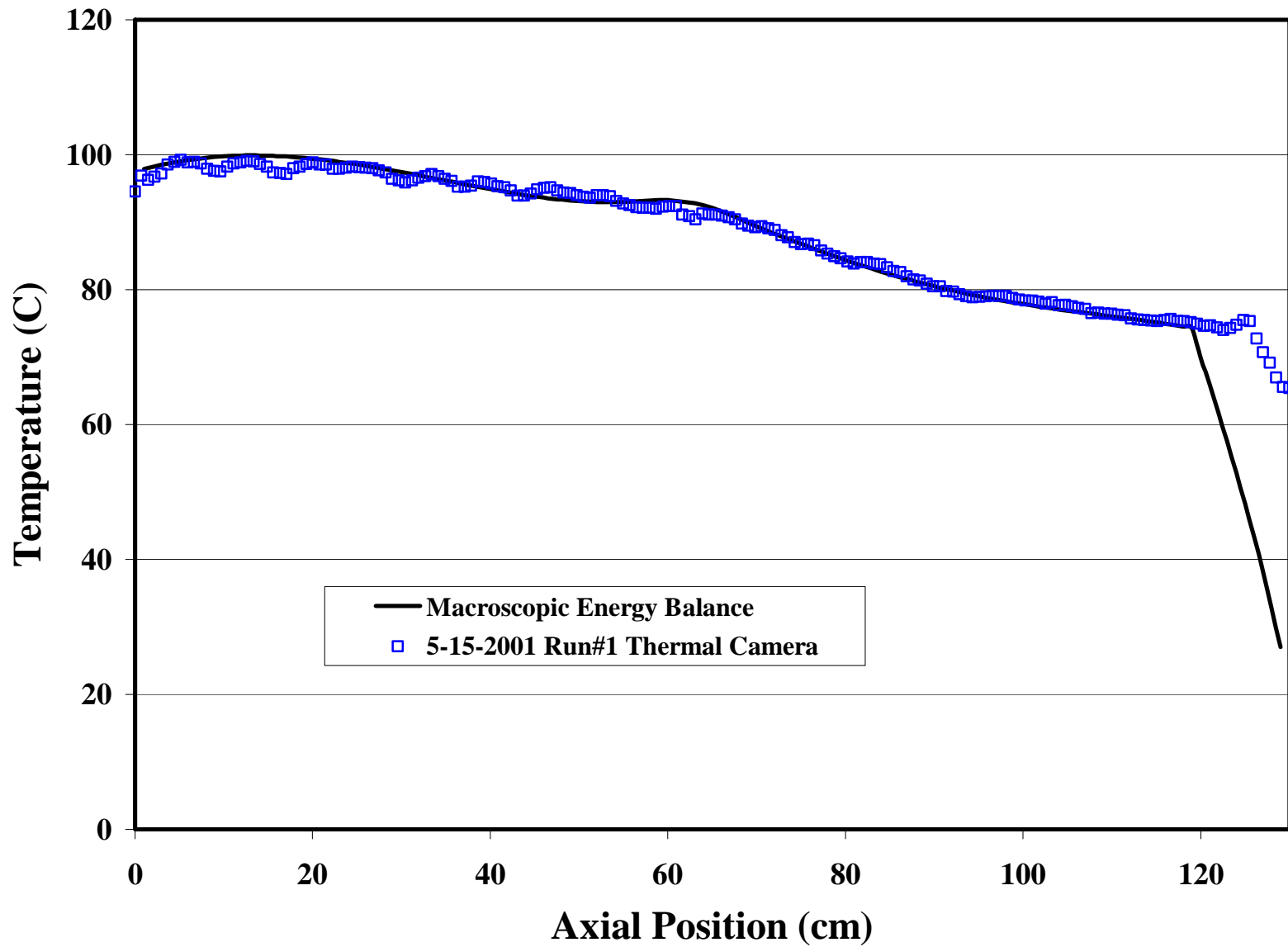


Figure 9

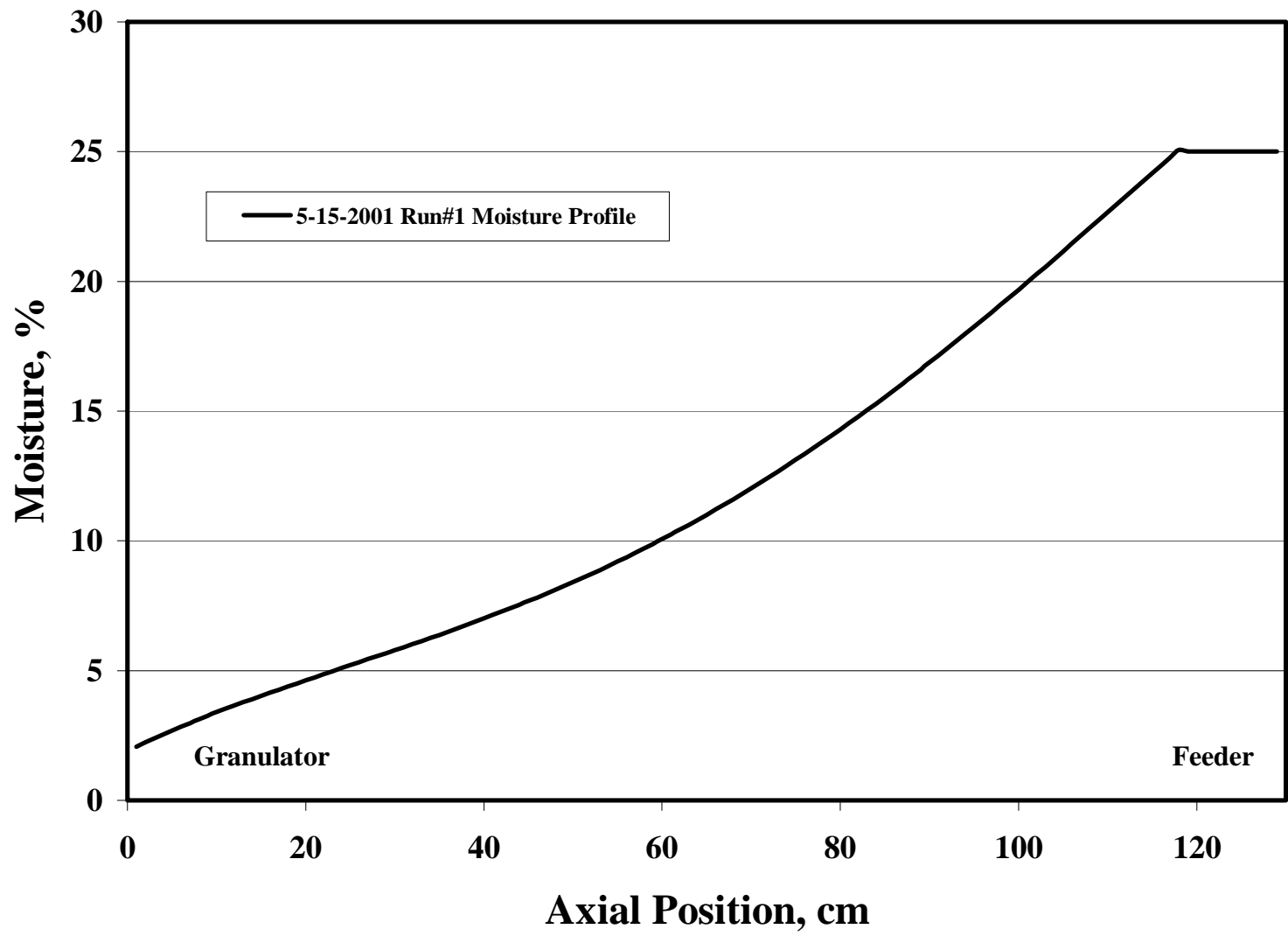


Figure 10